Chemical Engineering Journal 467 (2023) 143425

Contents lists available at ScienceDirect

Chemical Engineering Journal

journal homepage: www.elsevier.com/locate/cej

Mechanistic reaction micro-kinetics-based structure–activity relationships for palmitic acid hydrodeoxygenation over $NiMoS_x/Al_2O_3$ catalysts

Matej Žula [a,b], Miha Grilc [a,b], Blaž Likozar [a,c,d,e,*]

[a] Department of Catalysis and Chemical Reaction Engineering, National Institute of Chemistry, Hajdrihova 19, SI-1001 Ljubljana, Slovenia
[b] University of Nova Gorica, Vipavska 13, SI-5000 Nova Gorica, Slovenia
[c] Pulp and Paper Institute, Bogišićeva 8, 1000 Ljubljana, Slovenia
[d] Faculty of Polymer Technology, Ozare 19, SI-2380 Slovenj Gradec, Slovenia
[e] Faculty of Chemistry and Chemical Technology, University of Ljubljana, Večna pot 113, SI-1000 Ljubljana, Slovenia

ARTICLE INFO

Keywords:
Kinetics
Hydrodeoxygenation
Fatty acids
Mechanisms of hydrodeoxygenation

ABSTRACT

The kinetics of palmitic acid hydro-deoxygenation over sulfided $NiMo/\gamma\text{-}Al_2O_3$ have been described, including the gas–liquid–solid mass transport/surface chemistry in a magnetically-stirred batch reactor *via* temperature (225–275 °C), hydrogen pressure (30–70 bar) and catalyst loading (0.1–0.4 g) variation. Intermediates, the hexadecanol and palmityl palmitate, have been probed for a deeper physical understanding of mechanisms. Rates were used to show the impact of the continuum H_2 thermodynamic phenomena, availability and coverages on the selectivity among the direct hydrogenation, hydrogenolysis and decarbonylation reactions through the role of $H^{\bullet}$ formation dependent and independent changes. The system was reduced to 11 catalytic transformation steps, including 8 different molecular species, present in medium. Sequence is simulated to happen on the calculated functional number of active site structures, the activity of which was averaged, while the activation of H_2 was supposed to initiate independently. The results of model integrate parameters, such as energies, constants and performance. Process was highly temperature-related, while H_2 presence expressed linearly. Phases were characterized with temperature-programmed desorption analysis, coupled with mass spectrometry (TPD–MS) technique, transmission- (TEM), scanning electron microscopy (SEM), X-ray powder diffraction (XRD).

Table of abbreviations

The used notation was collected and described in Table 1.

1. Introduction

The hydrotreatment of lipids is one of the technologies that could reduce the societies dependence on fossil fuels and in this way slow down the increase of the amount of carbon in the carbon cycle. The goal of hydrotreatment is to use hydrogen from renewable sources to transform triglycerides to alkanes, which can later be upgraded with the current technologies to fuels and chemicals such as per example isomerization to renewable diesel, isomerization and hydrocracking into jet-fuel [1,2], the polymerization of alkenes to lubricants [3], production of light olefins [4] and numerous other options [5]. For hydrotreatment catalysts a number of metals are currently being tested but so far, there are three catalysts that are being used the most in the literature; those are platinum-based catalysts [6–9], nickel-based catalysts [10–12] and sulfided nickel molybdenum catalysts [13–17]. While all forms are quite active all also include significant short-comings [18]. Platinum being a very rare metal is very expensive and comes with a very high carbon footprint of 25.8–78.3 t CO_2e kg^{-1} [19]. Nickel catalysts usually suffer from low stability [20]. Sulfided NiMo catalyst on the other side require sulfide co-feeding and additionally require the removal of sulfur [4,13]. While the significant progress is being made with the nickel-based catalyst by combining them with oxophilic species such as W [21] or Zn [22], the sulfided NiMo catalysts currently offer the superior stability and activity which makes them a catalyst of choice for the industrial application of defunctionalization reactions [23,24].

The technology has found its place in most major oil & gas companies which are looking to both serve their more demanding customers and decrease their environmental impact in terms of carbon footprint. EU and US report to have 16 and 11 renewable diesel refineries respectively producing 5.5 and 6.6 billion liters per year [25,26]. To put the numbers into perspective US consumes about 500 million liters of diesel per day.

* Corresponding author.
E-mail address: blaz.likozar@ki.si (B. Likozar).

https://doi.org/10.1016/j.cej.2023.143425
Received 16 February 2023; Received in revised form 14 April 2023; Accepted 6 May 2023
Available online 8 May 2023

Table 1
Notation, symbols and units.

Notation	Description	Unit
μ	Dynamic viscosity of dodecane	mPa s
σ	Surface tension of dodecane	Nm
a	Area of gas–liquid interface	m^2
$C_{catalyst}$	Mass concentration of the catalyst in the mixture	g L^{-1}
$C_{H2,\ L}$	Molar concentration of hydrogen in the mixture	mol L^{-1}
$C_{H2,\ S}$	Concentration of hydrogen in the solid phase	mol g^{-1}
$C_{i,\ L}$	Concentration of a reaction component in the liquid phase	mol L^{-1}
$C_{i,\ S}$	Concentration of the adsorbed reaction component	mol
d	Diameter of the propeller	m
$D_{H2,\ DD}$	Diffusivity of hydrogen in dodecane	$m^2\ s^{-1}$
He	Henry's constant for hydrogen in dodecane	
k_{H2ads}	Constant of hydrogen adsorption on the catalyst	min^{-1}
k_{H2des}	Constant of hydrogen adsorption from the catalyst	min^{-1}
k_L	Gas transfer coefficient	
M_{dd}	Molecular mass of dodecane	g mol^{-1}
N	Stirring rate	min^{-1}
p	Measured pressure in the reactor vessel	bar
Re	Reynolds number	/
Sc	Schmitt number	/
Sh	Sherwood number	/
t	Time	min
V_L	Volume of the liquid phase	L
We	Weber number	/
ρ_{dd}	Density of dodecane	kg m^{-3}

The supply trends are highly dependable on the national policies but are expected to be increasing in the future. Beyond renewable diesel the sustainable aviation fuels (SAF) seem to be gaining a lot of traction with airlines looking to decrease the immense carbon footprint of commercial flying, the market value of SAF was only 480 million dollars in 2022 but is expected to exponentially grow in the future years. The technology leader in the field seems to be Neste oil with other oil companies such as Honeywell working parallelly in development and optimization of the processes to enable valorization of side products and lowering of the manufacturing cost to ease the competition of lipids with crude oil [27].

Ideally, active stable catalysts without any drawbacks would be used. To understand those drawbacks the in-depth understanding of mechanisms and kinetics seem like a crucial step. In light of that we have decided to try and explore the $NiMoS/Al_2O_3$ catalyst activity trough palmitic acid hydrodeoxygenation reactions to as accurately as possible describe the mechanisms and kinetics of the process.

The hydrodeoxygenation process is currently grouped in three parallel mechanisms (Fig. 1), hydrodeoxygenation (HDO), decarbonylation (DCN) and decarboxylation (DCX) reactions. They differ in the carbon balance, side products formation and hydrogen consumption.

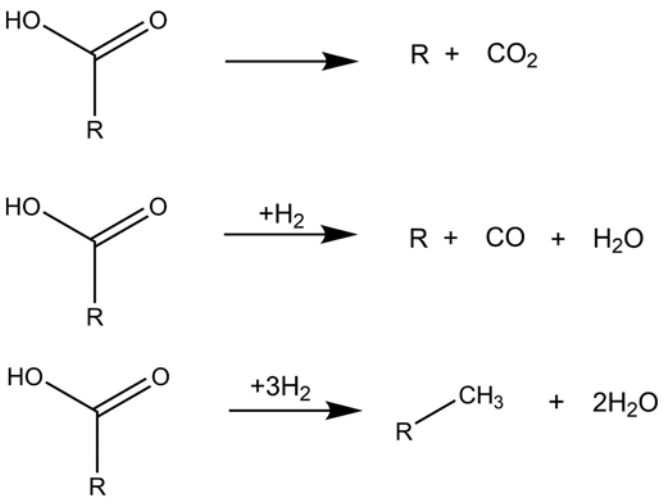

Fig. 1. Basic mechanisms of fatty acid hydrodeoxygenation.

The definitions of the difference between decarbonylation and decarboxylation differ from author to author and are relatively poorly defined. In this article the decarboxylation is defined as a reaction that requires no hydrogen in the mass balance but is however not able to be run under N_2 atmosphere. There are numerous estimates that consider the difference between decarboxylation and decarbonylation which are usually determined through the water–gas shift reaction equilibria [23,24]. However, Wagenhofer et al. [24] proposed the existence of a secondary indirect carbon oxide elimination. The topic therefore requires additional research to be properly clarified.

The selectivity between hydrodeoxygenation and decarbonylation/decarboxylation is one of the parameters which is usually reported, there are currently two trains of thought one is optimizing the selectivity for the optimal direct hydrodeoxygenation to avoid the production of carbon oxides which are usually associated with the extra pollution, can undergo methanations and can have a negative effect on the activity of noble metal catalysts, the other is for the system to undergo complete decarboxylation without requiring the presence of the hydrogen which technically enables a low cost solution due to lowering materials and equipment cost and decreasing the safety hazards of hydrogen use. Noble metals most often favor decarbonylation (DCN). Currently the literature says that higher temperature and neutral supports favor the DCN reactions while the more acidic supports and lower temperatures favor the HDO reactions [18]. Importantly, the noble metals catalysts have already been developed that can transform fatty acid selectively via HDO route [8,28]. Furthermore, Luo et al. [29] developed a Ru_3Sn_7/SiO_2 catalyst that can selectively transform fatty acids to fatty alcohols which was achieved with the addition of Sn which optimizes the adsorption of fatty acids while the dehydration and esterification reactions are suppressed due to low acidity.

Deoxygenation of fatty acids over sulfided NiMo catalyst is relatively independent of fatty acid concentration in the liquid phase and was previously even described with 0 order kinetics by Pimenta et al. [30]. In the Langmuir-Hinshelwood kinetic model that means that the constant of adsorption–desorption equilibrium is relatively high (5.14×10^{-2} for stearic acid [23]). There are two reaction intermediates - fatty alcohols and fatty aldehydes. Loosely depending on reaction conditions fatty aldehydes appear in very low concentrations. One of the reasons is their high activity [23] the other could be that the fatty aldehydes have a hard time desorbing from the surface thus, the subsequent reaction is more likely than desorption [24]. Fatty alcohols are usually dehydrated over Lewis acidic sites forming alkenes which can be further hydrogenated to alkanes. However, a dehydration to the ethers has previously not been reported for NiMoS catalysts at the HDO conditions. Parallel to hydrodeoxygenation the esterification reactions occur, which are usually linked to lower temperatures where the fatty acid and fatty alcohol can coexist over longer period of time [31]. In this article we will describe the kinetics of the palmitic acid hydrodeoxygenation including gas–liquid mass transfer of hydrogen, adsorption of the reactive species to the surface and the surface reaction kinetics.

2. Experimental

2.1. Materials

Palmitic acid (Acros organics, reagent grade, 98%), hexadecanol (Sigma-Aldrich, analytical standard), hexadecanal (Biosynth, >95%), pentadecane (Fluka, analytical standard), hexadecane (Fluka, analytical standard), palmityl palmitate (Sigma, >99%), dodecane (TCI, >99%), hexane (>98.5%, Merck), dimethyl disulfide (DMDS) (Sigma-Aldrich, >99%), $NiMo/Al_2O_3$, hydrogen (Messer, 5.0), nitrogen (Messer, 5.0).

2.2. Experimental work

The experimental work was done on batch Parr series 5000 Multiple Reactor system with the volume of 75 mL with magnetic stirring. Unless

specified differently, 1 g of palmitic acid, 0.25 g of the sulfided NiMo/Al_2O_3 catalyst and 30 g of dodecane were put in the reactor. The reactor was sealed and the oxygen was removed using nitrogen gas. Then the reactor was pressurized with H_2 and the reaction started. The used temperature range was between 225 and 275 °C and the initial pressures were between 30 and 70 bar. Temperatures and pressures for modeling were recorded automatically. The samples at 0 min were determined theoretically while all others were obtained by the following procedure: first the 2 mL vials were weighted. The sampling line was washed with about 0.5 mL of reaction mixture. Approximately 1 mL of filtered (PTFE filters) sample was then taken and sample in the vial was then again weighted. Due to poor solubility of palmitic acid and hexadecanol at room conditions the weighted sample was then diluted in 1 mL of hexane and weighted again. Diluted samples were then analyzed with gas chromatography (GCMS–QP 2010 Ultra, Shimadzu, Kyoto, Japan) equipped with a nonpolar column (Zebron ZB–5MSi, length 60 m, diameter 0.25 mm, film thickness 0.25 μm). Compounds were identified by MS (mass spectrometry) and quantified by FID (flame ionization detector). Importantly, the GC split ratio was kept at 20 due to palmitic acid being undetectable at lower concentrations at higher split ratios. The concentrations were determined using external standards with a 5 – point calibration method. The FID response of alkenes was assumed to be the same as the one from the alkanes with the same chain length. The experimental errors were determined from the repetition of the middle experiment (250 °C 50 bar H_2 and 0.25 g_{cat}) and applied as a relative error to other graphs.

2.3. Catalyst properties and activation

The commercially available NiMo/Al_2O_3 catalyst was activated by sulfidation. The process included drying at 200 °C over night, dried catalyst was sulfided in the batch reactor using 15 g of the catalyst, 3 g of DMDS and 20 mL of hexane at 350 °C for 90 min at the initial H_2 pressure of 25 bars. The excess H_2S was caught in the KOH bath.

The catalyst was previously characterized in the work of Grilc and Likozar [32] the results of which are presented in Table 2.

XRD, SEM and TEM analysis were done for the purpose of this work to both show and understand the catalyst structure. X-ray diffraction (XRD) patterns were characterized using PW3040/60 X'Pert PRO MPD diffractometer at 35 kV and 45 mA with Cu Kα radiation source (λ = 0.154056 nm) in the 2θ range from 10° to 80°, and using JCPDS database for reference. The catalyst surface was analyzed by field-emission scanning electron microscopy (FE-SEM) (SUPRA 35 VP, Carl Zeiss, Jena, Germany). Transmission Electron Microscopy analysis was conducted at 200 kV using a thermionic electron-source TEM JEOL model 2100.

Additionally, due to the smell of H_2S after the reaction which put into question the catalyst stability in the process and to expand the understanding of the catalyst functionality we have done the thermal pretreatment and ammonia TPD of our catalyst under the argon atmosphere. The thermal pretreatment was run for up to one hour under the flow of Ar (20 mL min^{-1}). While the ammonia TPD was run for about 100 min up to the 600 °C Molecular masses 17, 18, 28, 32, 34, 44, 64 were examined with the mass spectrometer.

2.4. Modeling

The potential of gas–liquid mass transport was described with Henry's law with the Henry's constant taken from the work by Gao et al. [33], the kinetics of transport were described with the Eq. (1).

$$\frac{dn}{dt} = k_L \times a \times \left(\frac{p}{He} \times \frac{M_{DD}}{\rho_{DD}} - C_{H_2L}\right) \tag{1}$$

k_L was calculated by Eq. (2) for magnetically stirred reactor [34] and also fitted on the global data.

$$\frac{k_L \times a}{V_L \times D_{H_2,DD}(T)} = 1.5 \times 10^{-4} \times Re^{1.45} \times Sc^{0.5} \times We^{0.5} \tag{2}$$

Area was estimated as the curved surface of a cone with r = 1.7 × 10^{-2} m and L = 5 × 10^{-2} m which was in accordance with measurements at the ambient pressure and temperature. Some inaccuracies might appear due to rather high viscosity change in light of the temperature increase however we believe the order of magnitude of the result is correct.

The diffusivity of hydrogen in dodecane ($D_{H_2,DD}$) was obtained from the work by Matthews et. al. [35] and viscosity (μ) and density (ρ_{DD}) of dodecane were obtained from the work of Koller et. al. [36], Reynolds, Schmidt and Weber number were obtained by Eqs. (3)–(5).

$$Re = \frac{\rho_{DD} \times N \times d^2}{\mu} \tag{3}$$

$$Sc = \frac{\mu}{\rho_{DD} \times D_{H_2,DD}(T)} \tag{4}$$

$$We = \frac{N^2 d^3 \rho_{DD}}{\sigma} \tag{5}$$

The mass balances for hydrogen and reactive components in the liquid and on the catalyst are defined with Eqs. (6)–(9). The $C_{i,S}$ is calculated in mols.

$$\frac{dC_{H_2,L}}{dt} = -k_{H_2ads} \times C_{H_2,L} \times C_{cat} + k_{H_2des} \times C_{H_2,S} \times C_{cat} + \frac{k_L \times a \times \left(\frac{p}{He} \times \frac{M_{DD}}{\rho_{DD}} - C_{H_2L}\right)}{V_L} \tag{6}$$

$$\frac{dC_{i,L}}{dt} = -k_{ads} \times C_{i,L} \times \frac{C_{FreeAS}}{C_{AS}} + k_{des} \times \frac{C_{i,S}}{V_L} \tag{7}$$

$$\frac{dC_{H_2,S}}{dt} = k_{H_2ads} \times C_{H_2,L} - k_{H_2des} \times C_{H_2,S} \pm r_i \tag{8}$$

$$\frac{dC_{i,S}}{dt} = k_{ads} \times C_{i,L} \times V_L \times \frac{C_{FreeAS}}{C_{AS}} - k_{des} \times C_{i,S} \pm r_i \tag{9}$$

These equations show that we assumed the adsorption surface for hydrogen to be unlimited at the current reaction conditions which is sync with the current knowledge of hydrogen adsorption and experimental results [23], while the adsorption of reactive components is limited with the number of active sites. Additionally, only one kind of active sites was presumed in the model while both the literature and the experimental results suggest that the adsorption sites for the deoxygenation and hydrogenation of double bonds might be different, however considering the amount of alkenes is low throughout the experiments done in the hydrogen atmosphere and that there to the best of our knowledge are no methods that could reliably measure the active sites we have assumed that there is only one kind of active sites which can bind any functional group (acids, esters, aldehydes, alcohols and double bonds). Additionally, it was assumed that the adsorption

Table 2
Textural properties and composition of NiMo catalyst.

Catalyst	Metal content (wt%)	Active phase	Deoxygenation active sites (μmol m^{-2})	BET-Surface area (m^2 g^{-1})	Pore volume (cm^3 g^{-1})	Pore size (nm)
NiMo/Al_2O_3	3/15	$NiMoS_x$	0.3	170	0.471	8.9

constant of all species with carbonyl group have the same adsorption constant, while the adsorption constant of the alcohols was measured by doing the dehydration reaction in the nitrogen atmosphere in the presence of palmitic acid. The adsorption constant of molecules with double bonds was assumed to be the same as the adsorption constant of carbonyl group molecules.

Chemical reactions were only considered to take place on catalyst surface while any homogeneous reactions were considered insignificant which is in line with current literature on modeling of fatty acid hydrodeoxygenations reactions. All chemical reactions took one of the following forms:

$$r_i = k_i \times C_{i,S} \times C_{H_2,S} \tag{10}$$

$$r_i = k_i \times C_{i,S} \tag{11}$$

$$r_i = k_i \times C_{i,S} \times C_{j,S} \tag{12}$$

The temperature dependence of the reaction rate was described with Arrhenius equation (Eq. (13)).

$$k(T) = k(523K) \times e^{\frac{-Ea}{R}\left(\frac{1}{T}-\frac{1}{523}\right)} \tag{13}$$

The reaction network was comprised of 11 catalytic reactions (Fig. 2). The reactions were based on our previous work [18], work by Hočevar et al.[37] and the work of Wagenhofer et al. [24]. Palmitic acid is a main reactant which can either hydrogenate or undergo decarboxylation. Hydrogenated palmitic acid transforms to hexadecanal which again can undergo decarbonylation into pentadecene or gets hydrogenated to hexadecanol. Hexadecanol further undergoes dehydration to hexadecene. Palmityl palmitate was one of the major intermediates which was described with formation via dehydration reaction between adsorbed palmitic acid and hexadecanol or via reaction between hexadecene and palmitic acid on the catalyst. Palmityl palmitate either degrades to hexadecanol and hexadecanal or to pentadecane and palmitic acid.

To improve clarity of the model and prevent confusion we have collected all of the rate expressions in the Table 3.

The rate and adsorption constants were calculated using the least square approximation method using the Nedler-Mead and Levenberg-Marquardt algorithms to determine the relevant kinetic parameters. In Eq. (14) the EXP, nS and nC represent the different experiments, samples and compounds respectively.

$$f(k_n, Ea_n) = \sum_{j=1}^{EXP}\sum_{i=1}^{nS}\sum_{C=1}^{nC}\left(C_{j,i}^{exp} - C_{j,i}^{mod}\right)^2 \tag{14}$$

The kinetic parameters 95% confidence intervals were also determined via Levenberg-Marquardt algorithm.

Internal diffusion was estimated by the effectiveness factor using the Thiele modulus following the similar procedure of Wagenhofer et al. [24]. The procedure is more accurately described in the SI.

Table 3
Rate expressions.

Rate expression	Name of the reaction
$r_{HL\_PA} = -k_{HL\_PA} \times C_{PA,S} \times C_{H_2,S}$	Hydrogenolysis of PA
$r_{H\_HAL} = -k_{H\_HAL} \times C_{Hal,S} \times C_{H_2,S}$	Hydrogenation of hexadecanal
$r_{DCX} = -k_{DCX} \times C_{PA,S}$	Decarboxylation
$r_{DHY} = -k_{DHY} \times C_{Hol,S}$	Dehydration of hexadecanol
$r_{EST} = -k_{EST} \times C_{PA,S} \times C_{Hol,S}$	Esterification
$r_{HL\_PP} = -k_{HL\_PP} \times C_{PP,S} \times C_{H_2,S}$	Hydrogenolysis of palmityl palmitate
$r_{H\_Hene} = -k_{H\_Hene} \times C_{Hene,S} \times C_{H_2,S}$	Hydrogenation of hexadecene
$r_{H\_Pene} = -k_{H\_Pene} \times C_{Pene,S} \times C_{H_2,S}$	Hydrogenation of pentadecene
$r_{DCN} = -k_{DCN} \times C_{Hal,S}$	Decarbonylation of aldehyde
$r_{DCN\_PP} = -k_{DCN\_PP} \times C_{PP,S} \times C_{H_2,S}$	Carbon scission of esters
$r_{EST\_Hene} = -k_{EST\_Hene} \times C_{PP,S} \times C_{H_2,S}$	Esterification of hexadecene and PA

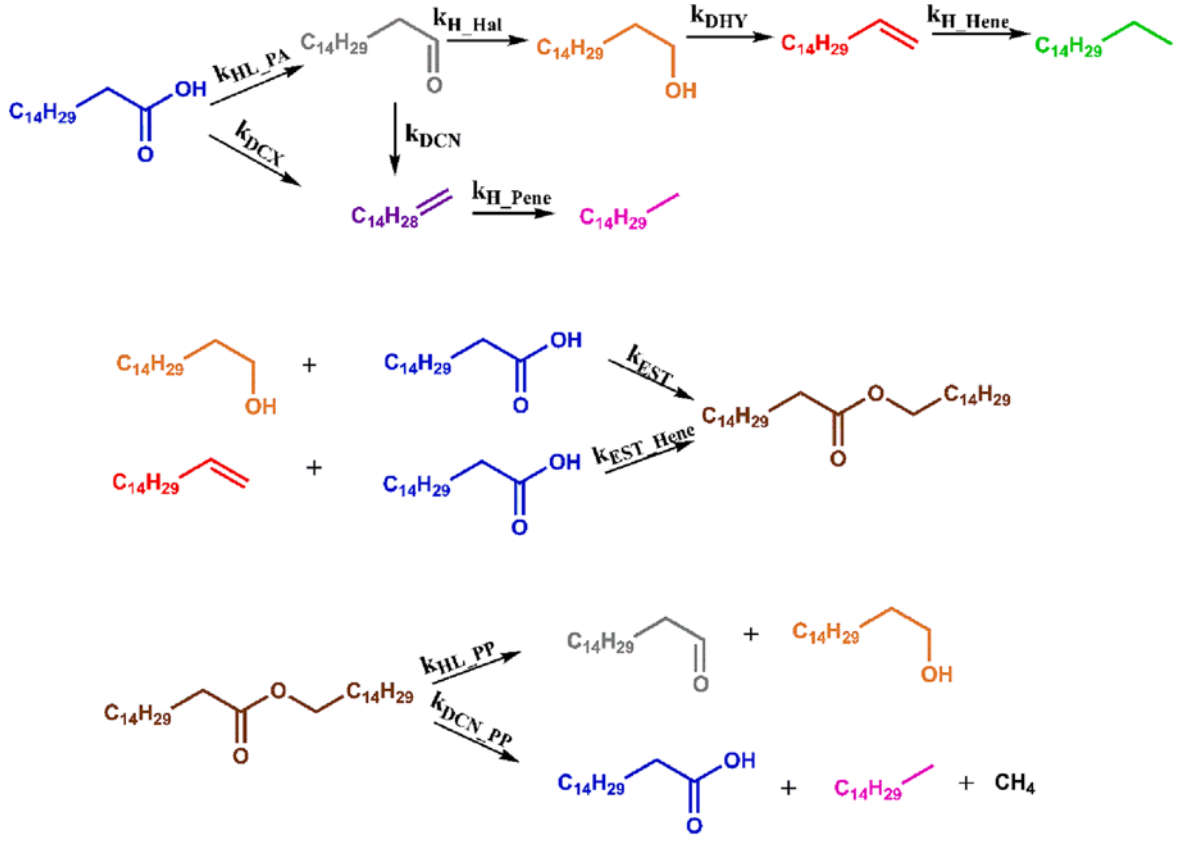

Fig. 2. Reaction scheme used for the modeling of the experiments, the color scheme is used in the graphs in the Results and discussion chapter.

3. Results and discussion

3.1. Catalyst characterization results

The XRD spectra (Fig. 3) of the catalyst was taken to examine the crystal structure of the catalyst, the peaks of three crystal structures-NiO, MoS_2, γ-Al_2O_3 were identified by the XRD scanning. The two major peaks at 45-46° and at 67° belong to γ-Al_2O_3 the support [38], the wide peak between 30 and 40° combines two peaks the peaks at 32°, 39° and 59° were identified to belong to the hexagonal MoS_2 species [38] while the peak between them at 36° belongs to the NiO species [38] which probably oxidized during the storage in the air atmosphere, Ni species can however efficiently reduce at temperature around 250 °C [39] which means that the oxidation should not impact the activity too harshly. The broader peaks indicate smaller particles with amorphous structure, typical for γ-Al_2O_3 which is structured via linkage of ~5 nm particles [40]. The broad peaks for MoS_2 indicate that the particles are quite amorphous without ordered structure, which is the desired outcome since the amorphous structure maximizes the amount of edges and vacant sites that are the most catalytically active [41].

SEM analysis was done revealing that the image of surface structure in 10^{-8}-10^{-4} m scale. It shows that the particles are indeed smaller than 100 μm with the majority being about 10 or less μm, while the "broken" sharp edges are probably the consequence of mechanical crushing. The macropores 10–100 nm are clearly visible in the Fig. 4b) (yellow circles) as black holes on the particle while the resolution was too low to observe any smaller pores. In the Fig. 4b) we can observe that particles include many ~20 nm structures such as bulges which probably enable its relatively high active surface area and subsequent catalytic activity.

Elemental analysis (SEM-EDX) was done for the surface of the particles (Fig. 5), while the resolution is not sufficient to show things such as coverage in the atomic resolution it can be seen that catalytic particles are homogeneously and uniformly covered by loaded metals and sulfur even though the sulfur was added post catalyst synthesis. All of the expected elements coverage can be seen in Fig. 6. Some catalytic materials such as P and Pt were also observed with EDX. It is likely that the P was added to improve the catalyst activity while the Pt was probably spotted due to the machine's over-sensitivity to Pt. The catalyst included some carbon deposits which were probably due to atmospheric impacts.

3.2. TEM

TEM analysis has been done on the catalyst, in a Fig. 7 below the catalyst particle is shown. The multiple ordered structures were spotted on the catalyst which have with elemental analysis corresponded to MoS_x particles, however in combination with XRD results these seem to be hexagonal MoS_2. Presumably, the one marked with red is MoS_2 tile seen from a vertical perspective, being thin enough for the Al_2O_3 not to distort the picture. The structures marked with blue circles are presumably the MoS_x structures seen from the side. Ni was not spotted by the TEM analysis presumably due to particles being too small for analysis.

3.3. NH_3-TPD and catalyst behavior at high temperatures

During the thermal pretreatment a number of MS (Fig. 8) peaks appeared, water and ammonia desorbed throughout the experiment reaching the peak at about 150 °C. Additionally, the sulfur species desorbed above 250 °C majorly in the form of SO_2. The results indicate that the smell after the reaction could be due to reduction of released SO_2 species to H_2S species in the hydrogen atmosphere.

The ammonia TPD was done after the thermal treatment and has shown two major peaks at around 100 and 400 °C. The major peak was deconvoluted into four peaks (Fig. 9). Other than NH_3 the released molecules included SO_2, H_2O and CO_2. The CO_2 is most likely the consequence of carbon deposits from the environment while the SO_2 and H_2O probably come from the remnants of the catalyst synthesis. The calculated amount of acid sites was 0.18 mmol g^{-1} (62.9 °C), 0.28 mmol g^{-1} (95.2 °C), 0.31 mmol g^{-1} (150.4 °C), 0.45 mmol g^{-1} (235 °C) which combined estimates the concentration of acidic sites to 1.22 mmol g^{-1}. The acidic sites were however not used as active sites in the model.

3.4. The kinetic parameters

We have calculated the kinetic parameters the combination of which offers an adequate description of the experimental data. Five groups of reactions are present on the catalyst under hydrogen atmosphere in the temperature range between 225 and 275 °C – hydrogenolysis, carbon–carbon scission, dehydration, esterification and hydrogenation reactions. The system included 8 major chemical species, palmitic acid, hexadecanal, hexadecanol, palmityl palmitate, hexadecene,

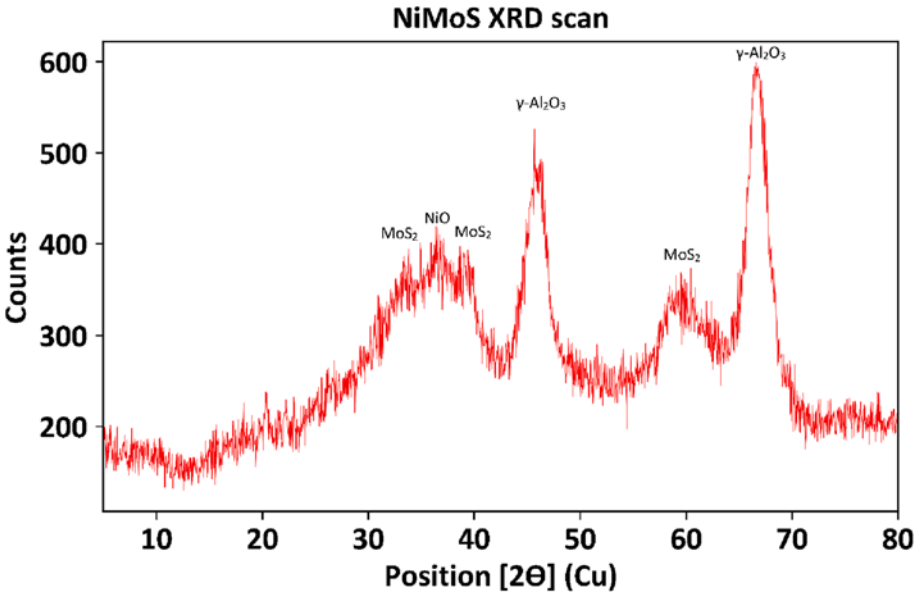

Fig. 3. XRD diffractogram of the catalyst.

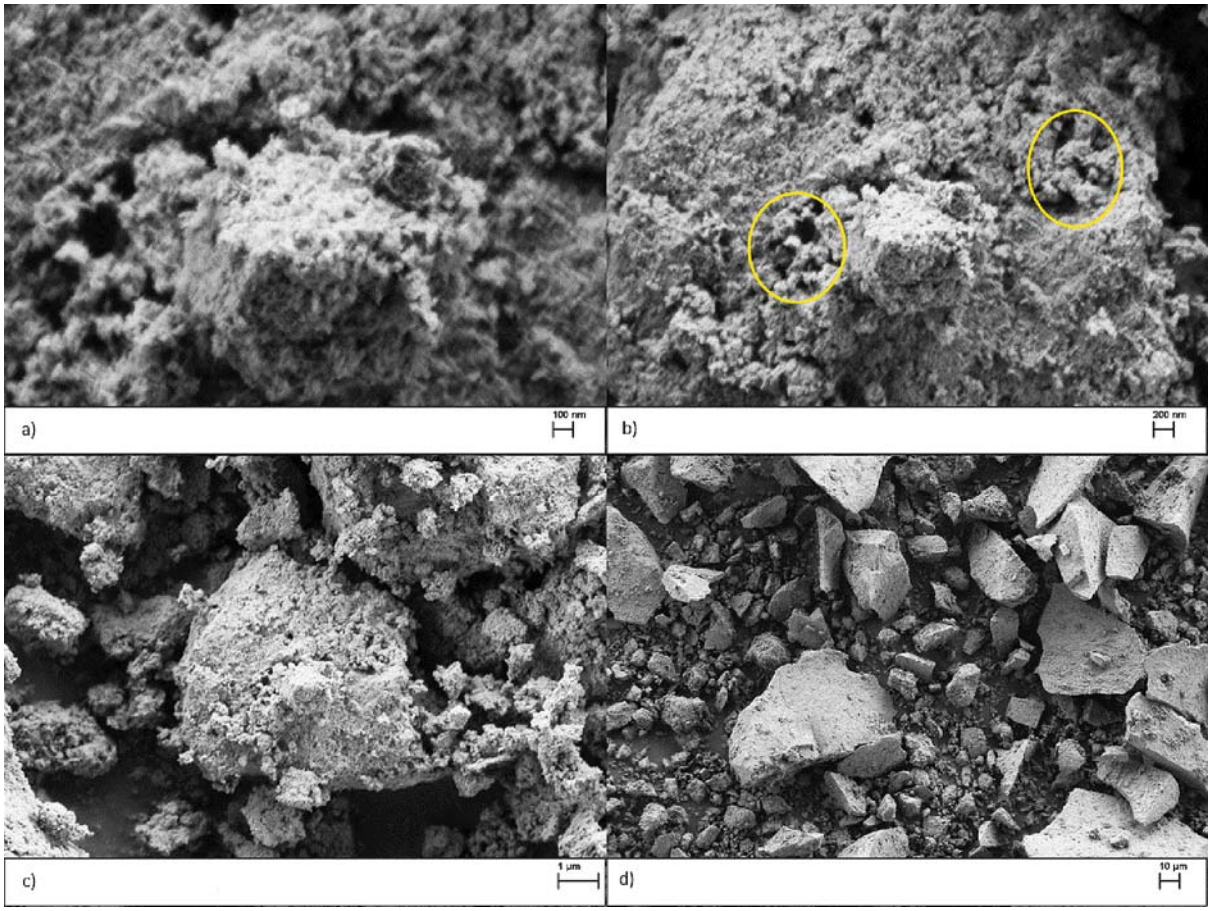

Fig. 4. SEM images of the catalyst.

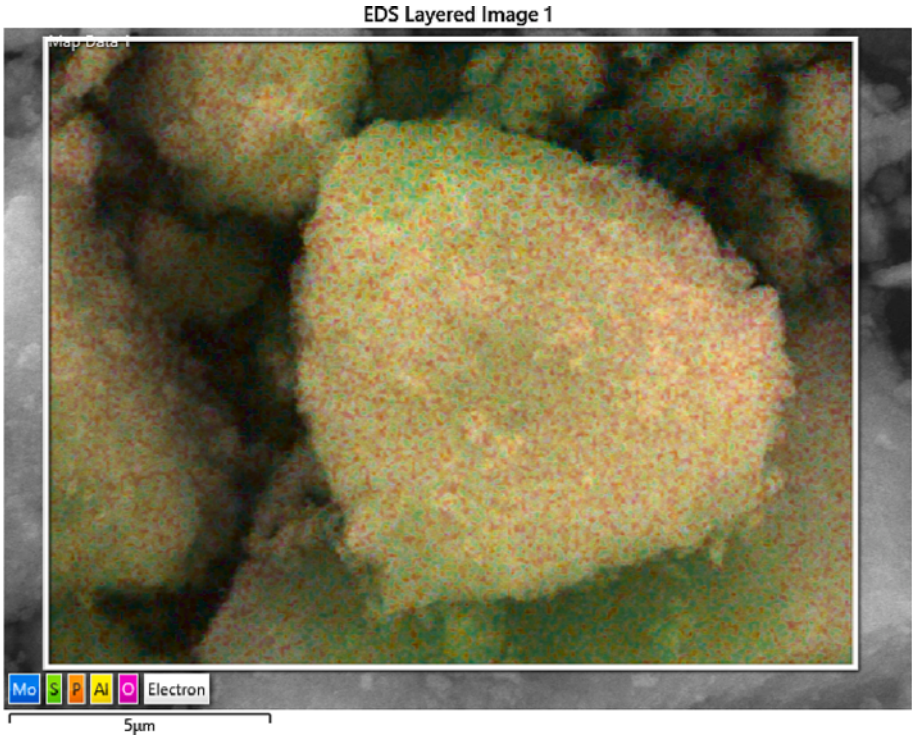

Fig. 5. SEM-EDX scan of the catalyst particle.

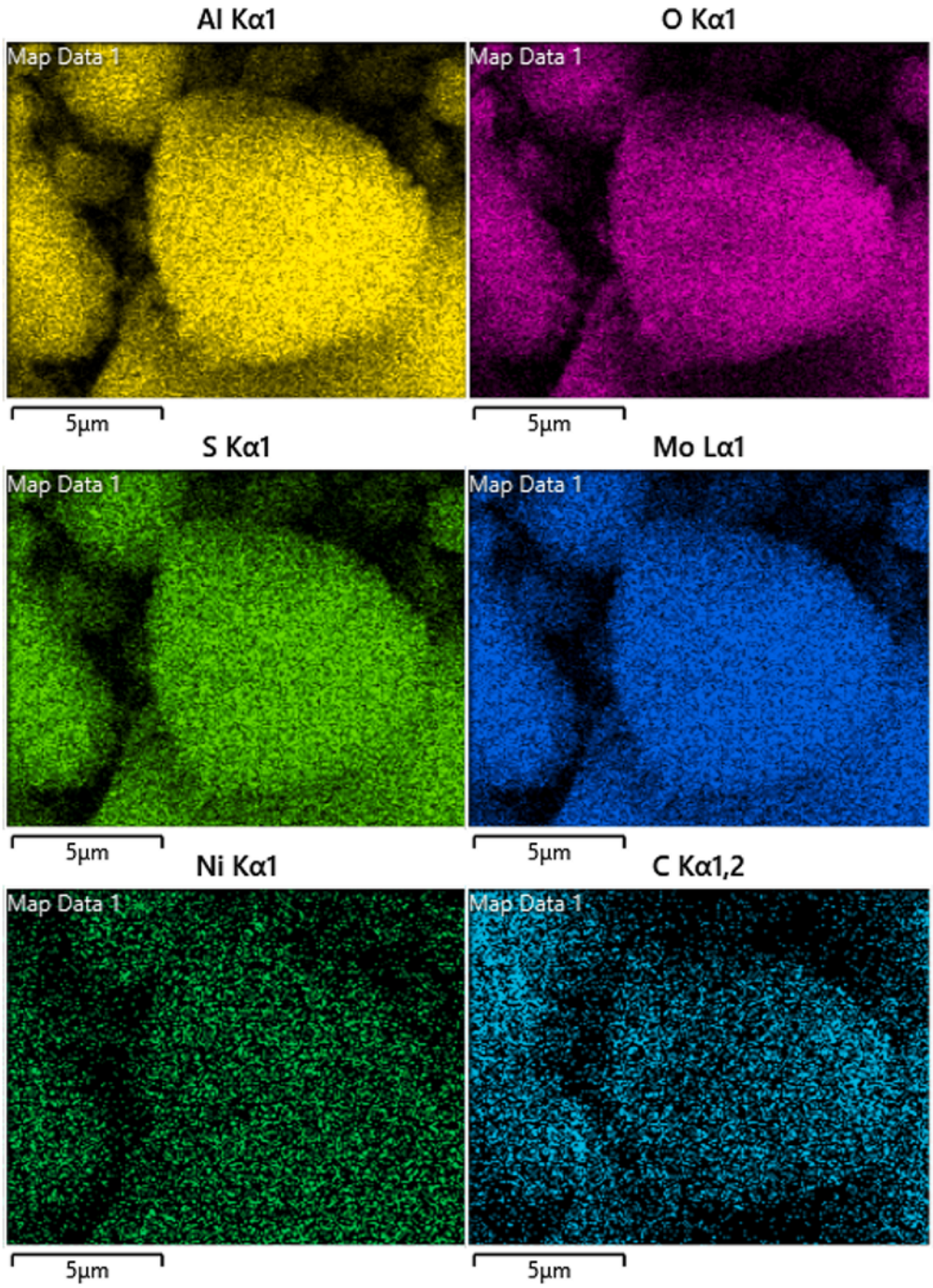

Fig. 6. SEM-EDX mapping for the key elements.

pentadecene, hexadecane and pentadecane. While the modeling in literature is most often described with the Langmuir-Hinshelwood kinetics, we used a different kinetics model, as described in the modeling chapter our model is designed to separate gas, liquid and solid phase which are connected via gas–liquid mass transfer and liquid–solid mass transfer (adsorption). The advantages of such model are in a high potential for the very accurate representation of events that actually occur on the catalyst such as competitive adsorption, sequential reaction without desorption etc.. While the drawbacks can include a poor fit due to inadequate understanding of the processes and inadequate understanding of the events occurring on the catalyst. Thus, such modelling is very useful to in a way stress test our understanding of the processes, illuminate the gaps and offer some answers which can be hidden in the combination of rate and adsorption constants in the Langmuir-Hinshelwood model. The results of the model include all of the calculated parameters which are presented in Table 4.

3.5. *The dependence of reaction rate on temperature.*

The reactions were highly dependent on the temperature which is due to high energy activation of hydrogenolysis of palmitic acid (Ea_{HL_PA} = 93.6 kJ mol^{-1}) and decarboxylation (Ea_{DCX} = 156.1) which are the only transformations that PA can undergo alone over the sulfided NiMo/γ-Al_2O_3. The obtained values are in agreement with the literature [23,24]. Dehydration of hexadecanol has also shown a high dependence on temperature variation (Ea_{DHY} = 87.6). Hydrogenation of double

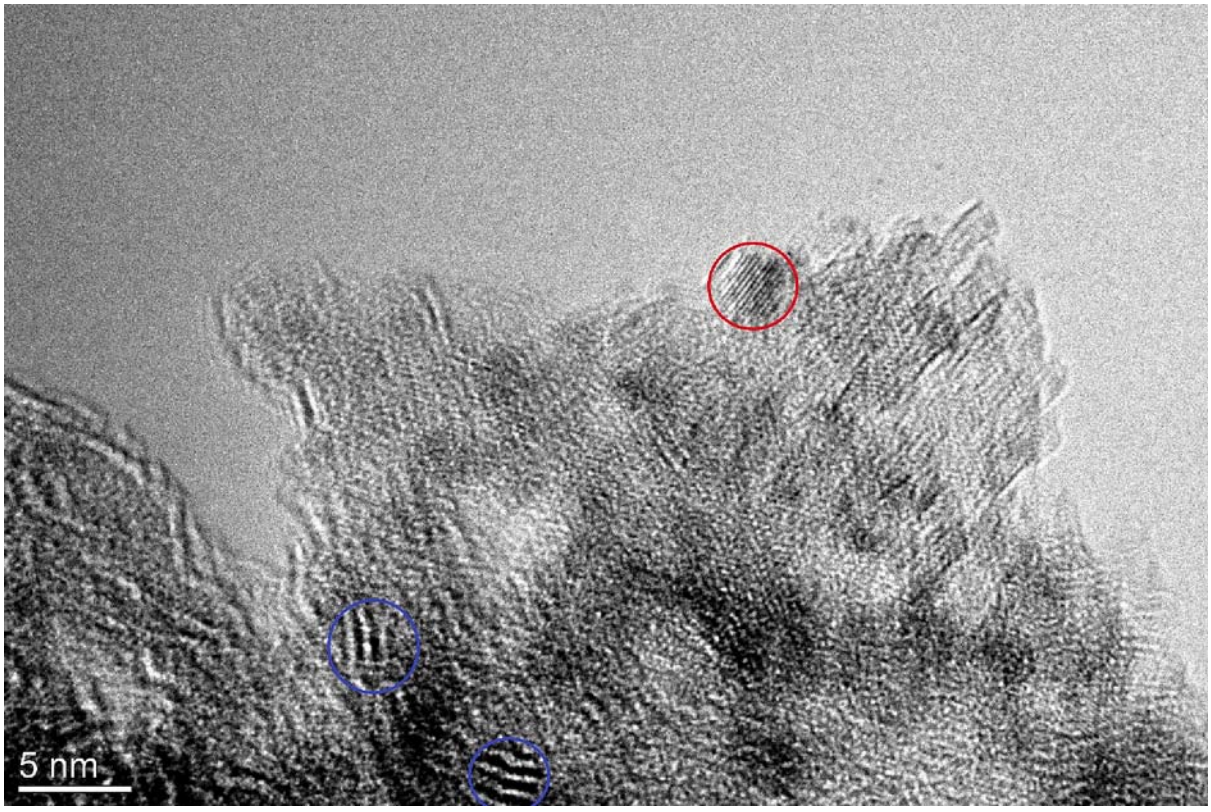

Fig. 7. TEM picture of the catalyst with visible geometry associated with MoS_2 catalytic sites.

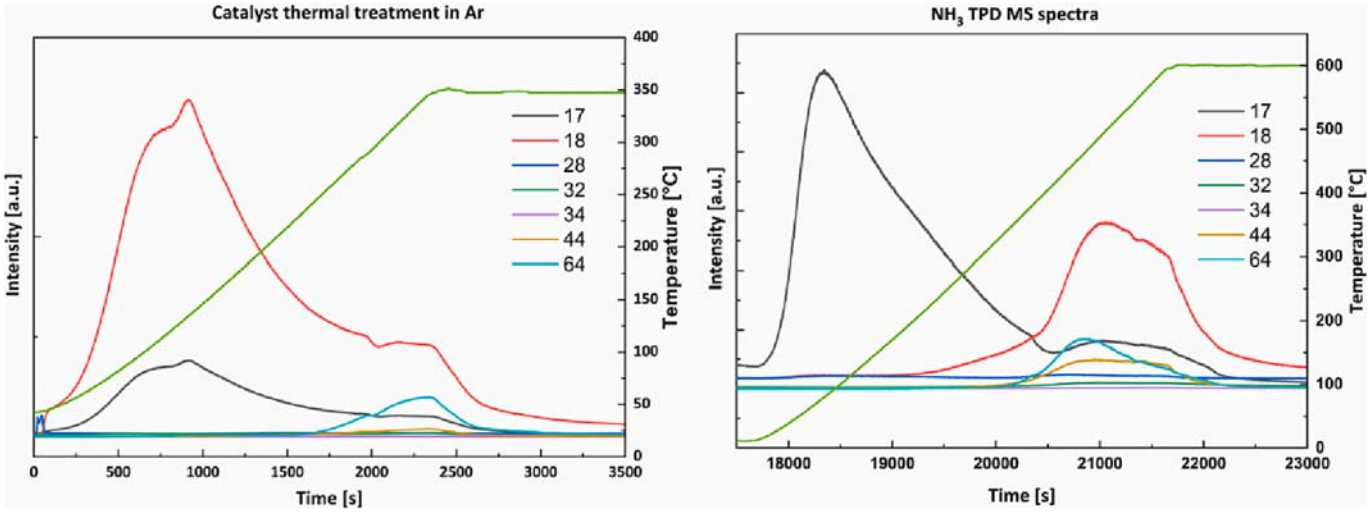

Fig. 8. The thermal pretreatment and NH_3-TPD gas evolution profile obtained with MS analysis. Each line represents the molecular mass in the legend. The rising green line is the temperature profile. (For interpretation of the references to color in this figure legend, the reader is referred to the web version of this article.)

bonds activation energies are about 25 kJ mol^{-1} which is about 10 kJ mol^{-1} higher than the results from Hočevar et al. [42]. The palmityl palmitate hydrogenolysis and decarbonylation were much less dependent on the temperature (Ea_{HL_PP} = 34.7 kJ mol^{-1} and Ea_{DCN_PP} = 59.0 kJ mol^{-1}) however its deoxygenation was slower probably because of the worse accessibility of the active sites for the large molecule with an ester functional group. In short, the reactions were highly dependent on the temperature and the temperature increase improves the reaction rates significantly – at the chosen conditions more than any other tested parameter (Fig. 10).

3.6. The dependence of reaction rate on pressure.

In Fig. 11 we can see the reaction rate change with the change in the initial hydrogen pressure, four initial pressures were probed, 0, 30, 50 and 70 bar. No conversion was observed for 0 bar initial pressure. The other have as expected shown linear dependence of hydrogen pressure, which shows that the hydrogen availability on the catalyst is one of the rate limiting factors. Additionally, even carbon–carbon scission reactions that have shown no dependence on hydrogen pressure at higher pressures have shown no conversion while no hydrogen was present. The selectivity for HDO was the function of hydrogen pressure gradually

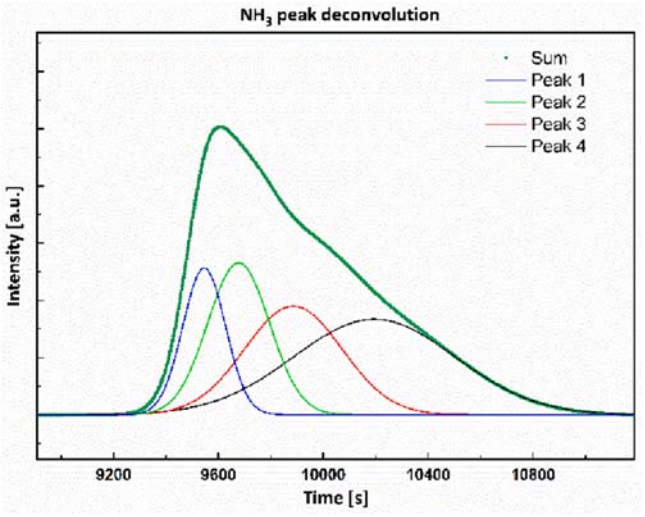

Fig. 9. The deconvolution graph showing all 4 described peaks.

Table 4
Modeling results.

Mass transfer parameters			
Parameter	**Value**	**Unit**	**Description**
k_L fitted	1.29×10^{-5}	m s^{-1}	Fitted on global set of data
k_L calculated	1.46×10^{-5}	m s^{-1}	Calculated by Eq. (2)
a	0.0029	m^2	Estimated area of gas–liquid interface during mixing.
k_{ads}	$>1 \times 10^4$	min^{-1}	Constant of adsorption for reactive species.
k_{des}	$>4 \times k_{ads}$	min^{-1}	Constant of desorption for reactive species.
$k_{ads\_Hexadecanol}$	$k_{ads} \times 0.104$	min^{-1}	Constant of adsorption for hexadecanol.
k_{ads_H2}	12.6	min^{-1} g_{cat}^{-1} L	Constant of adsorption for hydrogen.
$k_{\_des\_H2}$	15.6×10^3	min^{-1} g_{cat}^{-1} L	Constant of desorption for hydrogen.

Kinetic results			
index (i)	**k_i [min^{-1} g_{cat} mol^{-1}] (T = 523 K)**	**Ea [kJ mol^{-1}]**	**Description**
HL_PA	$30 \pm 1 \times 10^2$	93 ± 8	Hydrogenolysis of PA
H_Hal	$26 \pm 7 \times 10^4$	88 ± 24	Hydrogenation of hexadecanal
DCX	$43 \pm 20 \times 10^{-3}$ [a]	156 ± 72	Decarboxylation
DHY	20.9 ± 5.8 [a]	85 ± 40	Dehydration of hexadecanol
EST	$44 \pm 28 \times 10^4$ [b]	78 ± 39	Esterification
HL_PP	$24 \pm 5 \times 10^2$	24 ± 20	Hydrogenolysis of palmityl palmitate
H_Hene	$16 \pm 5 \times 10^3$	29 ± 23	Hydrogenation of hexadecene
H_Pene	$23 \pm 5 \times 10^3$	25 ± 21	Hydrogenation of pentadecene
DCN	18 ± 4[a]	114 ± 31	Decarbonylation of aldehyde
DCN_PP	$15 \pm 10 \times 10^1$	59 ± 47	Carbon scission of esters
EST_Hene	$15 \pm 13 \times 10^4$ [b]	32 ± 15	Esterification of hexadecene and PA

For [a] the units change to min^{-1} and for [b] the units change to min^{-1} mol^{-1}.

increasing towards C_{16} products. The increase in conversion with the increase of the hydrogen pressure can be seen clearly in Fig. 11 and is in accordance with the literature [20,23,43]. The model describes the conversion of palmitic acid well; however, it becomes more inaccurate for the prediction of the intermediates concentration at lower conversion. The reason for that is every reaction was considered to be separate, meaning it is impossible in the model for the palmitic acid to transform directly to per example hexadecene without becoming hexadecanal and hexadecanol first. The formed molecule does not necessarily have to desorb but this means that the results are relatively sensitive to change in adsorption/desorption rates and ratios. The graphs in Fig. 11 show that the increase in pressure has impacted the reaction rate rather linearly. The errors at 30 bar experiment seem significant due the bottom part of the graph being significantly zoomed in.

3.7. Formation and deoxygenation of intermediates.

We will start from the bottom and work our way upwards, therefore the dehydration of alcohols seems to be an appropriate place to start. Hočevar et al. [37] have presumed two types of alcohol deoxygenation dehydration and hydrogenolysis, they have theoretically shown that the dehydration is the main mechanism due to lower energy of activation (65 kJ mol^{-1} and 115 kJ mol^{-1} respectively) however we have shown that the hydrogenolysis was undetectable for hexadecanol (Fig. 12a), b)). The major mechanism of alcohol deoxygenation is thus dehydration, importantly, dehydration requires no hydrogen presence and presumably happens on acidic catalytic sites. The hexadecanol is transformed to most likely 1-hexadecene which can further undergo structural isomerization forming a wide array of hexadecenes which were identified on MS by the maximum molecular mass of 224, showing a number of peaks (around 4–5) indicating strong isomerization activity of the catalyst however those peaks eventually disappear due to hydrogenation activity of the catalyst. The rate of dehydration did not show a strong dependence on whether the hexadecenes were further hydrogenated to hexadecanes which indicates that the hexadecenes have a lower impact on the rate of adsorption of hexadecanol than the PA and other oxygenates as can be seen from the graphs a) and b) on Fig. 12. On the other hand, all of the oxygenated species do compete with hexadecanol for the catalytic spots (on the Fig. 12 the results of the hexadecanol dehydration in the presence of the PA (Fig. 12 c)), the results show that the dehydration function of the catalyst is significantly impaired in the presence of the PA and formed palmityl palmitate. We believe that is because of the preferential adsorption of PA and palmityl palmitate on the catalytic sites. The model indicates that the palmitic acid is 6.3 times more likely to adsorb on the catalytic sites than the hexadecanol. Other oxygenates were presumed to be as likely to adsorb on the catalytic sites as the PA. Additionally, the results indicate that the hexadecanol dehydration can behave differently in the hydrogen atmosphere in the presence of PA, in such conditions the PA presence seems to further retard the dehydrogenation reactions beyond the adsorption preference and the model predicts a higher consumption of hexadecanol compared to experimental data. We presume that is because one of the formed products – either hydroxyls or carbon oxides formed during hydrogenolysis or carbon–carbon scission further retards the dehydration reactions. The effect subsides rapidly after the complete consumption of the PA (see Fig. 10), in the model we presume that the effect is the consequence of the CO formation during the C-C scission, which could fit due to low CO solubility which means that the formed CO is transported rather rapidly in the gas phase and as the formation stops the concentration of CO in the liquid phase should drop rapidly as well, however, because we did not model the CO transition to gas state and thus the impact of its formation might not be described perfectly. In isolation the sulfided NiMo/γ-Al_2O_3 has proven to be a very active dehydration catalyst with non-detectable activity towards oligomerization regardless of hydrogen presence.

Formation of esters especially over sulfided NiMo/γ-Al_2O_3 catalyst is rarely reported however, we believe that this is attributed to the fact the most of the studies use higher temperatures with relatively high catalyst loading which prevent formation due to lower concentrations of fatty alcohols. In Fig. 12c) we show that esterification in nitrogen atmosphere cannot be properly described with the same model which is expected considering the esterification reactions were not the focus of the study. The experiment however, clearly shows how palmitic acid presence

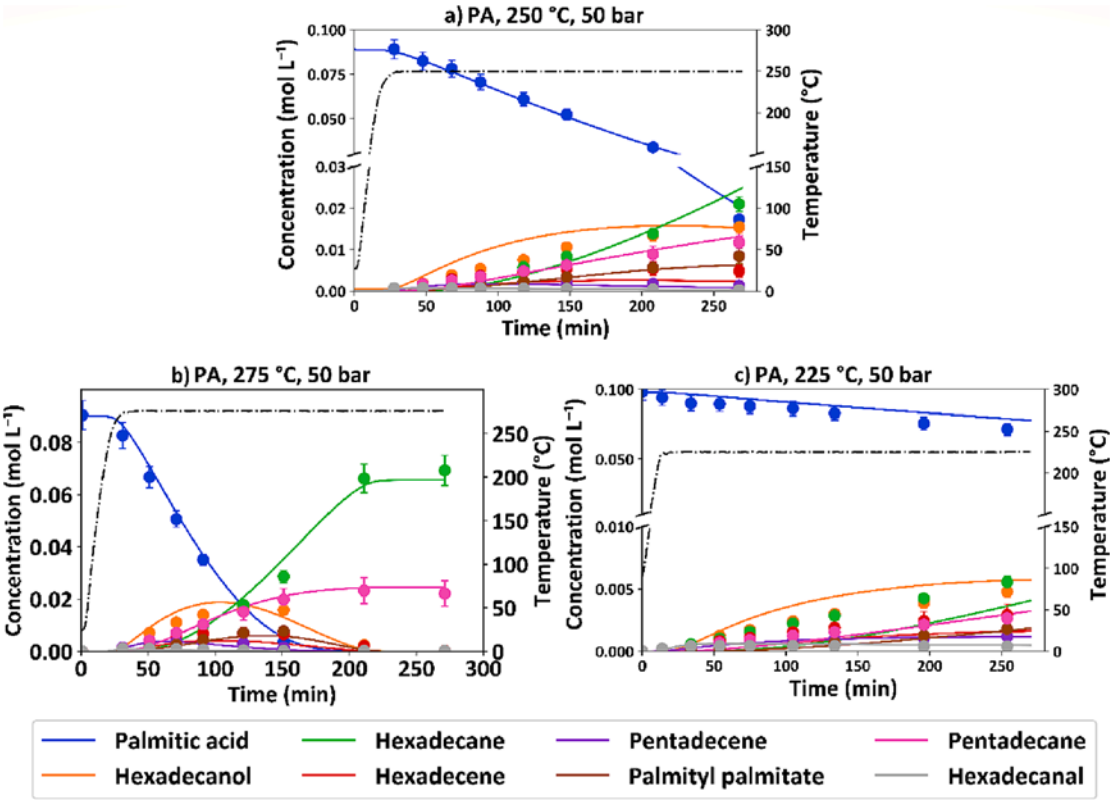

Fig. 10. The temperature variation experiments (dots) and model fits (lines). -· represents temperature profile. The graph at 225 °C is split in two parts to better show the results. The compounds can be identified by color.

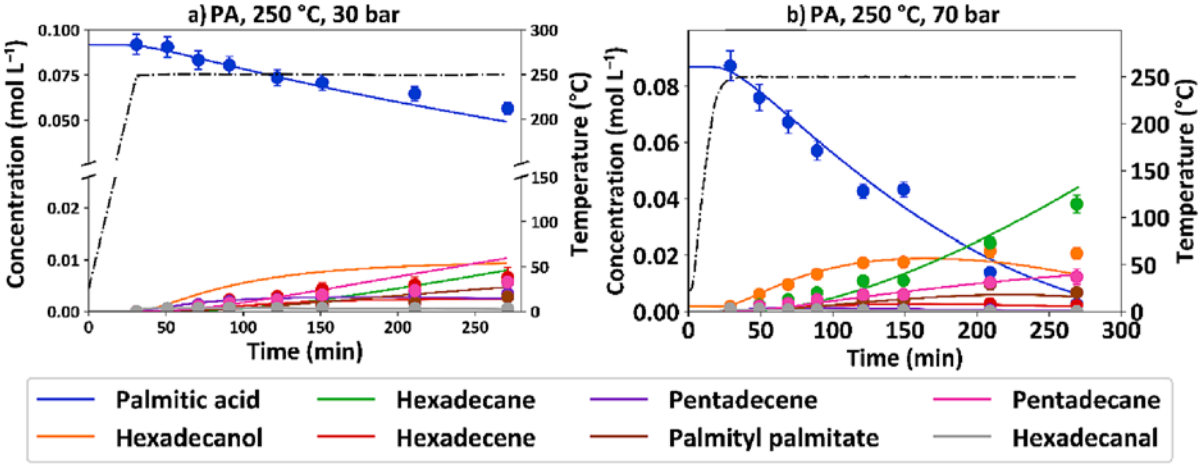

Fig. 11. The pressure variation experiments (dots) and model fits (lines). -· represents temperature profile. The graph a) at 30 bar H_2 is split in two parts to better show the results. The compounds can be identified by color.

reduces the rate of dehydration reactions and in combination with hexadecanol and hexadecene causes esterification but does clearly not undergo decarboxylation or decarbonylation reactions which is shown by the lack of C_{15} compounds in the system. Importantly, the alcohol undergoes oxidation to aldehyde in the system. To clarify deoxygenation of esters we have additionally done an experiment with the palmityl palmitate. In our experiment the palmityl palmitate has deoxygenated to two major products hexadecanol and hexadecane, presumably as the consequence of the hydrogenolysis of the C-OC bond forming hexadecanal and hexadecanol which can subsequently be quickly converted to hexadecanol and hexadecene. A higher than expected amount of C_{15} products was formed during HDO of palmityl palmitate which leads us to believe that the esters can be cleaved with C-C scission forming methyl palmitate and pentadecane. However, methyl palmitate was not among the detected products which is probably because of the fast scission of O-CH_3 bond. There is another possible reaction path that would be possible for ester hydrogenolysis – formation of hexadecane and PA. Such hydrogenolysis was neglected due to model including such reaction path offered worse results for the general fit and therefore indicated that such reaction path is very minor for the palmityl palmitate HDO. The activity of the catalyst for the ester hydrogenolysis was worse than for the PA hydrogenolysis (40% conversion compared to 70% for PA at 250 °C 50 bar H_2) which is reasonable considering the palmityl palmitate is a larger molecule and thus, could have harder time

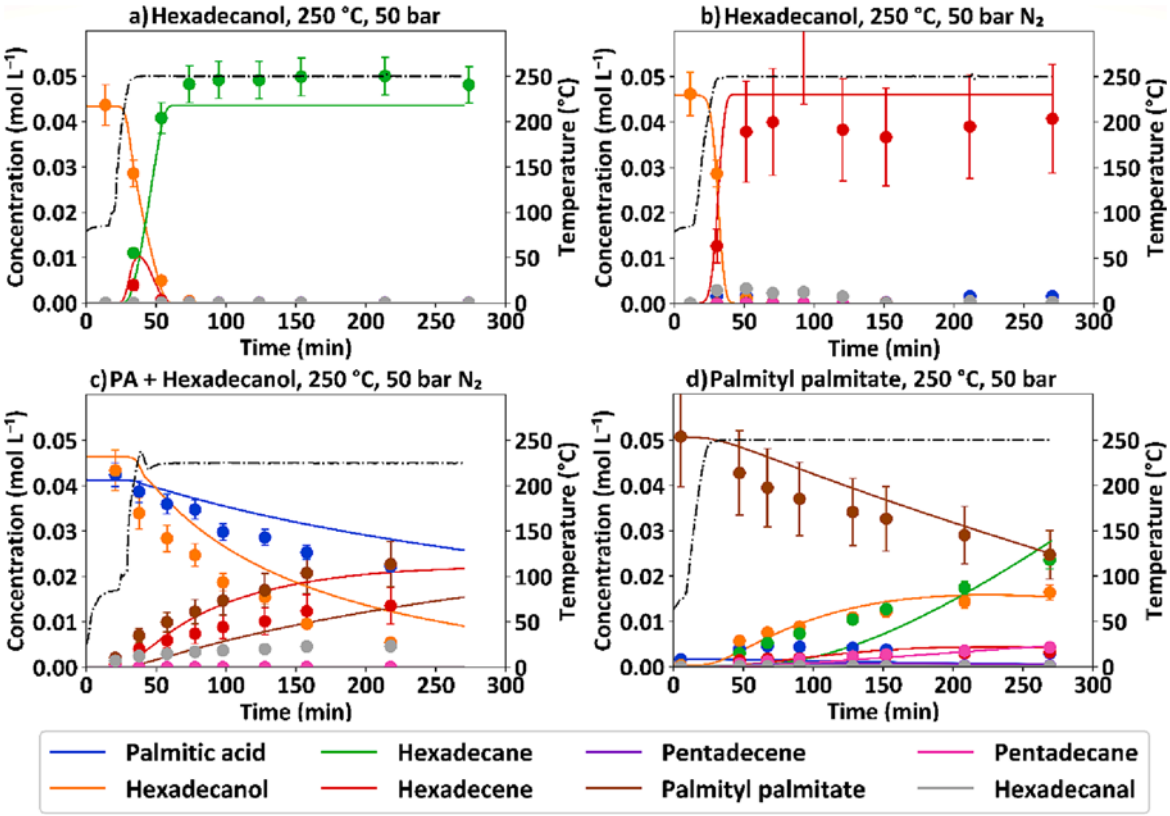

Fig. 12. Experiments with the intermediates (dots) and model fits (lines). -- represents temperature profile. The compounds can be identified by color.

accessing pores and the active sites in those pores. The formation is thus not a desired reaction path for the rapid deoxygenation and should be avoided by adaption of the catalyst synthesis or with the increase in the reaction temperature.

3.8. Mass transfer limitations

The mixing variation is usually used as a test how much of the impact the external mass transfer has on the reaction rate [23,42]. The test is based on the results of the few studies which show that the mass transport dependent rate should increase with the increase in the Reynolds number (mixing rate increase) [34,44]. We have done the same test and obtained results show that the impact of mixing variation was in the range of the experimental error. (See Fig. 13).

However, in addition we have done some additional experiments with different catalyst loadings (Fig. 14). The model predicts linear scaling of surface reaction rates with the concentration of adsorbed hydrogen which was confirmed by the experimental results (note: in the experiment with 0.1 g of catalyst the concentration of PA was normalized to fit the mass balance). Minor errors appear at lower catalyst loading however considering that the reaction rates and selectivity at the most intense process conditions (275 °C, 0.4 g_{cat}) is accurately predicted the mass transfer impacts should be negligent. Additionally, the kL calculated and the kL fitted fit with ~ 10% differential which is neglectable considering both constants were calculated completely independently and that the area of the interface was overly simplified. The calculated hydrogen concentration for the model was in the range between 1 and 5×10^{-4} mol g_{cat}^{-1} which is a similar concentration to the number of calculated deoxygenation active sites from the Table 2 (5.6×10^{-5} mol g_{cat}^{-1}), both were again determined completely independently.

We have additionally calculated the effectiveness factor for PA, hexadecanal and hexadecanol for the reaction at the most intense reaction conditions (275 °C) the procedure for the description is shown in the SI. In Fig. 15 we show the impact of the particle radius on the

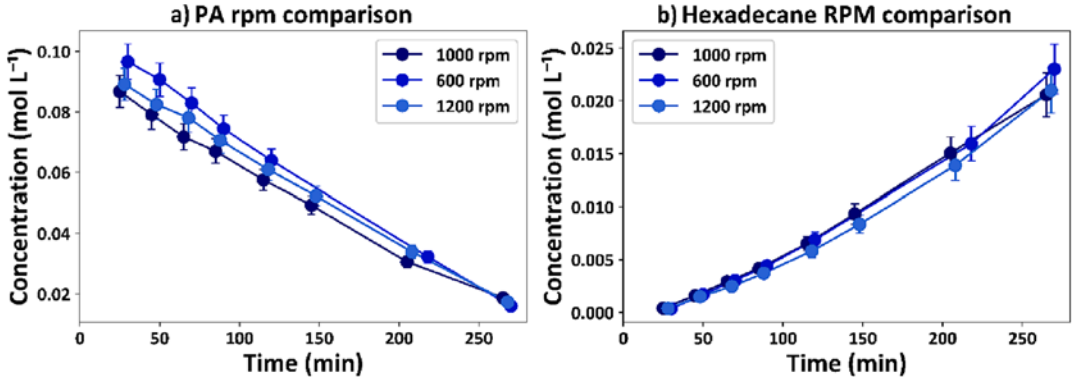

Fig. 13. The results of the rpm variation for the experiment at 250 °C and 50 bar H_2 pressure. The PA and hexadecane were chosen to show the variation.

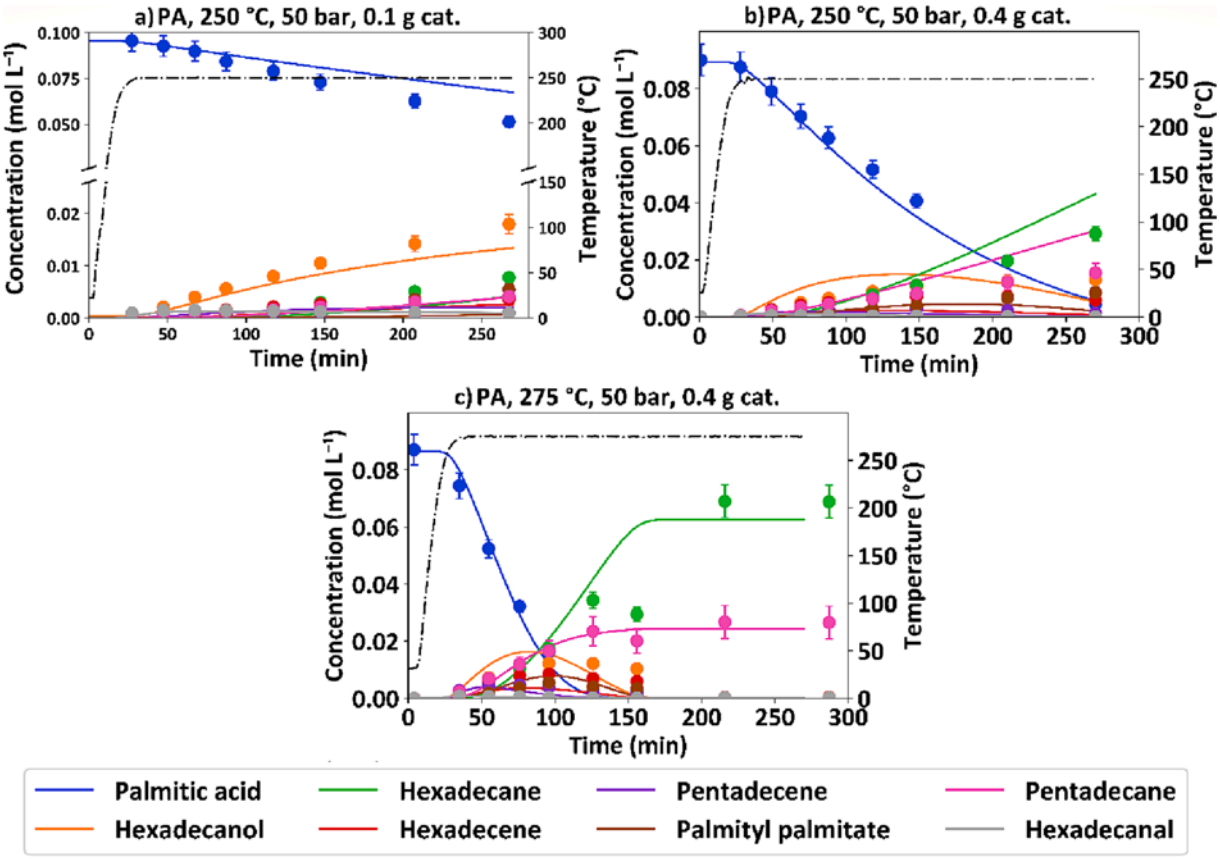

Fig. 14. The catalyst loading variation. The dots represent experimental concentration while the lines present the modeled results. The compounds can be identified by color.

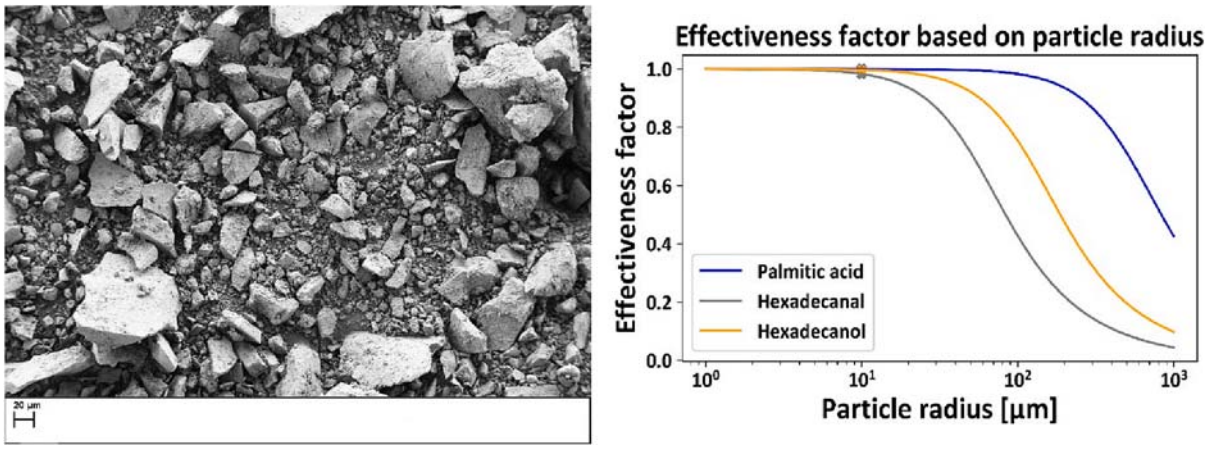

Fig. 15. The catalyst particles used in the experiment and on the right the graph representing the impact of the catalyst particle size on the effectiveness factor.

reaction rates. Consider however, that the hexadecanal and hexadecanol are in most cases intermediates which might not require a complete diffusion to the pore due to them being produced at the same active sites. Regardless, the calculated effectiveness factors were calculated to be $\eta > 0.95$ more accurately (0.99, 0.98 and 0.99 for the PA, hexadecanal and hexadecanol respectively (x on Fig. 15)), the catalyst particles were considered to be cylinders with radius of 10 µm. The effectiveness factor shows that the impact of the internal diffusion on the reaction rate is negligent. On the left part of the Fig. 15 the catalyst particles typically used in the experiment are shown.

3.9. *Overview of the kinetic results, simplifications and outlook*

The catalytic process can thus be described with the mechanism previously shown in Fig. 2. The major reaction pathways for sulfided NiMo/γ-Al_2O_3 are shown with bold arrows in Fig. 16. The catalyst has shown about 70% selectivity towards direct HDO compared to DCX and DCN selectivity. At used temperatures the formation of esters was shown to be significant probably due to relatively high concentration of present fatty alcohols. On the other hand, the reaction between present alkenes and fatty acids seems possible but minor due to alkenes concentrations being proportionally lower than the concentrations of fatty alcohols. The hydrogenation of alkenes has shown some dependence on the presence

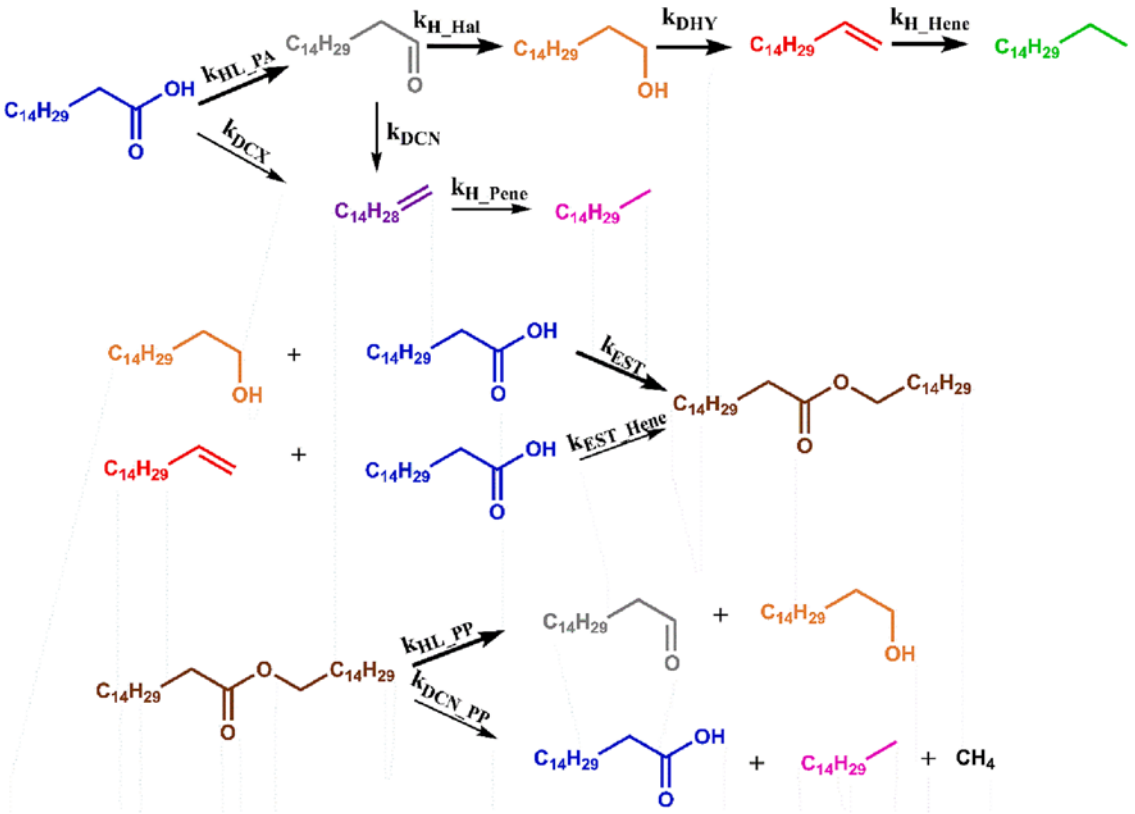

Fig. 16. The reaction mechanism, bold arrows show major reaction pathways.

of other oxygenates (the rate would significantly increase while the concentration of oxygenates was negligent) however, its impact on the rate of the deoxygenation process is hard to measure due to a number of effects present in the system, regardless it seems highly plausible that efficient hydrogenation enables rapid deoxygenation and that alkenes compete for the deoxygenation spots on the catalyst. As predicted in the model the presence of alkanes, be it end products (hexadecane, pentadecane) or the solvent dodecane seems to have no impact on the reaction rates beyond enabling efficient transfer of hydrogen from gas to liquid phase. The major deoxygenation path for esters seems to be the hydrogenolysis to fatty aldehyde and alcohol while the minor paths produce fatty acid and pentadecane presumably due to the hydrogenolysis of the C-CO bond.

The model assumes a few neglects and simplifications, in the gas phase hydrogen is assumed to be the only gas in the gas phase, the mass transfer is described with Henry's law where the liquid phase is assumed to be only dodecane rather than the mixture including PA and the catalyst. In the liquid phase all components excluding hexadecanol were presumed to have the same adsorption constant as the adsorption constants are currently not measurable for the such catalytic systems. All components except H_2 and alkanes were presumed to compete for the same catalytic spots which is quite unlikely, since we have even experimentally shown that per example the presence of hexadecene does not significantly decrease the dehydration rate of hexadecanol.

This model shows that there is more than PA competitive adsorption that blocks the dehydration of hexadecanol and hydrotreatment of palmityl palmitate – possibly the CO formed during the decarbonylation of PA, that is presumably why the errors appear at equimolar concentrations of oxygenates when the impact of palmitic acid adsorption should already subside. There seems to be an interplay on the deoxygenation sites which prevents the consumption of palmityl palmitate and hexadecanol beyond the linear impact of fatty acid concentration, therefore the model predicts that the hexadecanol and palmityl palmitate will be consumed quicker. We have also shown that the hexadecene does not significantly hinder the dehydration reactions and that the hydrogen presence has a negligible impact on the dehydration function of the catalyst, furthermore there seem to be no hydrogenolysis of the hexadecanol at the used experimental conditions which is often implied in the literature. Additionally, model shows that the reactions at the chosen conditions can be described with unlimited hydrogen adsorption where there is linear dependence of the hydrogen dependent reactions on the presence of hydrogen on the catalyst. The model should also be able to describe the reactions at conditions where hydrogen is not in such a strong excess however additional gases should be introduced into the gas phase and there might have to be some adaption for the description of the decarbonylation reactions at very low hydrogen pressures or at significant mass transfer limitations. Ideally, the model could be upgraded with additional experimental data such as more accurate adsorption description, types and stability of active sites but there are currently very limited experimental methods for the determination of the number and the accessibly of the catalytic sites especially for the sulfided catalysts and the big molecules in the liquid phase which are all interesting topics that we plan to tackle in our future work.

4. Conclusion

We modeled the mass transfer and the kinetics of the palmitic acid hydrodeoxygenation reactions, combined there were 8 compounds that were interlinked with 11 different reactions. The reaction mechanisms included hydrogenolysis, two types of carbon–carbon scission, dehydration, esterification and hydrogenation reactions. The reactions were modeled based on the variation of temperature (225–275 °C), hydrogen pressure (30–70 bar) and catalyst loading (0.1–0.4 g per 40 mL). To confirm mechanisms the additional reactions were done with different reactants such as hexadecanol in both hydrogen and nitrogen atmosphere, palmityl palmitate and the combination of palmitic acid and hexadecanol. The model predicts full conversion and product selectivity relatively well, however the errors can appear when multiple

oxygenated species are present in the reaction feed at close to equimolar concentrations.

Declaration of Competing Interest

The authors declare that they have no known competing financial interests or personal relationships that could have appeared to influence the work reported in this paper.

Data availability

Data will be made available on request.

Acknowledgements

This research was funded by the Slovenian Research Agency (ARRS) through Programme P2–0152 and the research projects J2-2492 and NC-0013.

Appendix A. Supplementary data

Supplementary data to this article can be found online at https://doi.org/10.1016/j.cej.2023.143425.

References

[1] J. Cheng, Z. Zhang, X. Zhang, Z. Fan, J. Liu, J. Zhou, Continuous hydroprocessing of microalgae biodiesel to jet fuel range hydrocarbons promoted by Ni/hierarchical mesoporous Y zeolite catalyst, Int. J. Hydrogen Energy 44 (23) (2019) 11765–11773, https://doi.org/10.1016/j.ijhydene.2019.03.073.

[2] Z. Zhang, J. Cheng, Y. Zhu, H. Guo, W. Yang, Jet fuel range hydrocarbons production through competitive pathways of hydrocracking and isomerization over HPW-Ni/MCM-41 catalyst, Fuel 269 (2020), 117465, https://doi.org/10.1016/j.fuel.2020.117465.

[3] S. Chen, T. Wu, C. Zhao, Conversion of lipid into high-viscosity branched bio-lubricant base oil, Green Chem. 22 (21) (2020) 7348–7354, https://doi.org/10.1039/d0gc01338b.

[4] P. Sun, S. Liu, Y. Zhou, S. Zhang, Z. Yao, Production of renewable light olefins from fatty acid methyl esters by hydroprocessing and sequential steam cracking, ACS Sustain. Chem. Eng. 6 (10) (2018) 13579–13587, https://doi.org/10.1021/acssuschemeng.8b03889.

[5] R. E. Peralta-Robledo, C. E. Santolalla-Vargas, F. Sanchez-Minero, V. Santes, S. O. Flores-Valle, O. Elizalde Solis, Effect of the formulation of Pd/γ-Al2O3+Pd/H-ZSM-5 catalysts prepared by mechanical mixing for the thermal and catalytic hydrotreating of castor oil, *Catal. Today*, 346(2018) (2020) 81–86, doi: 10.1016/j.cattod.2019.02.063.

[6] D. Jin, G. Ye, J. Zheng, W. Yang, K. Zhu, M.-O. Coppens, X. Zhou, Hierarchical silicoaluminophosphate catalysts with enhanced hydroisomerization selectivity by directing the orientated assembly of premanufactured building blocks, ACS Catal. 7 (9) (2017) 5887–5902, https://doi.org/10.1021/acscatal.7b01646.

[7] T.H. Kim, K. Lee, M.Y. Kim, Y.K. Chang, M. Choi, Effects of fatty acid compositions on heavy oligomer formation and catalyst deactivation during deoxygenation of triglycerides, ACS Sustain. Chem. Eng. 6 (12) (2018) 17168–17177, https://doi.org/10.1021/acssuschemeng.8b04552.

[8] A.V. Chistyakov, V.V. Kriventsov, A.V. Naumkin, A.Y. Pereyaslavtsev, P. A. Zharova, M.V. Tsodikov, Evolution of active ingredients and catalytic properties of Pt-Sn/Al2O3 catalysts in the selective deoxygenation reaction of vegetable oils, Pet. Chem. 56 (7) (2016) 607–615, https://doi.org/10.1134/S0965544116070045.

[9] S. Janampelli, S. Darbha, Selective deoxygenation of fatty acids to fuel-range hydrocarbons over Pt-MOx/ZrO2 (M = Mo and W) catalysts, Catal. Today 375 (2021) 174–180, https://doi.org/10.1016/j.cattod.2020.04.020.

[10] Z.Y. Jing, et al., Nickel catalysts on hydrodeoxygenation of fatty acid methyl esters to fuel-like hydrocarbons, Ranliao Huaxue Xuebao/J. Fuel Chem. Technol. 46 (4) (2018) 427–440, https://doi.org/10.1016/S1872-5813(18)30018-5.

[11] S. Ding, F. Li, Z. Li, H. Yu, C. Song, D. Xiong, H. Lin, Catalytic hydrodeoxygenation of waste cooking oil and stearic acid over reduced nickel-based catalysts, Catal. Commun. 149 (2021) 106235.

[12] F. Wang, J. Xu, J. Jiang, P. Liu, F. Li, J. Ye, M. Zhou, Hydrotreatment of vegetable oil for green diesel over activated carbon supported molybdenum carbide catalyst, Fuel 216 (2018) 738–746, https://doi.org/10.1016/j.fuel.2017.12.059.

[13] J. Hancsók, O. Visnyei, A. Holló, L. Leveles, A. Thernesz, G. Varga, J. Valyon, Alternative diesel fuels with high hydrogen content in their molecular structures, Renew. Energy 142 (2019) 239–248, https://doi.org/10.1016/j.renene.2019.04.105.

[14] S.A. El Khatib, S.A. Hanafi, Y. Barakat, E.F. Al-Amrousi, Hydrotreating rice bran oil for biofuel production, Egypt. J. Pet. 27 (4) (2018) 1325–1331, https://doi.org/10.1016/j.ejpe.2018.08.003.

[15] H. Ojagh, D. Creaser, M.A. Salam, E.L. Grennfelt, L. Olsson, The effect of rosin acid on hydrodeoxygenation of fatty acid, J. Energy Chem. 28 (2019) 85–94, https://doi.org/10.1016/j.jechem.2018.01.023.

[16] J. Hancsók, D. Sági, J. Valyon, Diesel fuel blending components from mixture of waste animal fat and light cycle oil from fluid catalytic cracking, J. Environ. Manage. 223 (June) (2018) 92–100, https://doi.org/10.1016/j.jenvman.2018.06.011.

[17] P. Arora, H. Ojagh, J. Woo, E. Lind Grennfelt, L. Olsson, D. Creaser, Investigating the effect of Fe as a poison for catalytic HDO over sulfided NiMo alumina catalysts, Appl. Catal. B Environ. 227 (January) (2018) 240–251, https://doi.org/10.1016/j.apcatb.2018.01.027.

[18] M. Žula, M. Grilc, B. Likozar, Hydrocracking, hydrogenation and hydrodeoxygenation of fatty acids, esters and glycerides: Mechanisms, kinetics and transport phenomena, Chem. Eng. J. 444 (2022) 136564.

[19] G.M. Mudd, Sustainability reporting and the platinum group metals: A global mining industry leader? Platin. Met. Rev. 56 (1) (2012) 2–19, https://doi.org/10.1595/147106711X614713.

[20] K. Jeništová, I. Hachemi, P. Mäki-Arvela, N. Kumar, M. Peurla, L. Čapek, J. Wärnå, D.Y. Murzin, Hydrodeoxygenation of stearic acid and tall oil fatty acids over Ni-alumina catalysts: Influence of reaction parameters and kinetic modelling, Chem. Eng. J. 316 (2017) 401–409, https://doi.org/10.1016/j.cej.2017.01.117.

[21] S. Xing, Y. Liu, X. Liu, M. Li, J. Fu, P. Liu, P. Lv, Z. Wang, Solvent-free hydrodeoxygenation of bio-lipids into renewable alkanes over NiW bimetallic catalyst under mild conditions, Appl. Catal. B Environ. 269 (2020) 118718, https://doi.org/10.1016/j.apcatb.2020.118718.

[22] M. Gousi, E. Kordouli, K. Bourikas, E. Simianakis, S. Ladas, G.D. Panagiotou, C. Kordulis, A. Lycourghiotis, Green diesel production over nickel-alumina nanostructured catalysts promoted by zinc, Catal. Today 355 (2020) 903–909, https://doi.org/10.1016/j.cattod.2019.02.034.

[23] P. Arora, E.L. Grennfelt, L. Olsson, D. Creaser, Kinetic study of hydrodeoxygenation of stearic acid as model compound for renewable oils, Chem. Eng. J. 364 (January) (2019) 376–389, https://doi.org/10.1016/j.cej.2019.01.134.

[24] M.F. Wagenhofer, E. Baráth, O.Y. Gutiérrez, J.A. Lercher, Carbon-carbon bond scission pathways in the deoxygenation of fatty acids on transition-metal sulfides, ACS Catal. 7 (2) (2017) 1068–1076, https://doi.org/10.1021/acscatal.6b02753.

[25] Renewable diesel, U.S. Department of Energy - Energy Efficiency and Renewable Energy Alternative Fuels Data Center, 2023.

[26] E. Voegele, EU demand for biodiesel, renewable diesel to remain flat in 2022, Biodiesel Magazine (2022).

[27] D. Kubička, Upgrading of lipids to hydrocarbon fuels via (hydro)deoxygenation, in: M. Crocker, E. Santillan-Jimenez (Eds.), Chemical Catalysts for Biomass Upgrading, Wiley, 2020, pp. 469–496.

[28] P.A. Zharova, A.V. Chistyakov, S.S. Shapovalov, A.A. Pasynskii, M.V. Tsodikov, Original Pt-Sn/Al2O3 catalyst for selective hydrodeoxygenation of vegetable oils, Energy 172 (2019) 18–25, https://doi.org/10.1016/j.energy.2019.01.084.

[29] Z. Luo, Q. Bing, J. Kong, J.Y. Liu, C. Zhao, Mechanism of supported Ru3Sn7 nanocluster-catalyzed selective hydrogenation of coconut oil to fatty alcohols, Catal. Sci. Technol. 8 (5) (2018) 1322–1332, https://doi.org/10.1039/c8cy00037a.

[30] J.L. Castagnari Willimann Pimenta, M. de Oliveira Camargo, R. Belo Duarte, O. A. Andreo dos Santos, L.M. de Matos Jorge, A novel kinetic model applied to heterogeneous fatty acid deoxygenation, Chem. Eng. Sci. 230 (2021) 116192, https://doi.org/10.1016/j.ces.2020.116192.

[31] L. Chen, G. Li, M. Zhang, D.a. Wang, S. Li, C. Zhang, X. Li, K.H. Chung, Preparation of reduced Ni-Nb-O composite hydrogenation catalysts for highly selective conversion of free fatty acids to n-alkanes, Fuel 282 (2020) 118842, https://doi.org/10.1016/j.fuel.2020.118842.

[32] M. Grilc, B. Likozar, Levulinic acid hydrodeoxygenation, decarboxylation and oligmerization over NiMo/Al2O3 catalyst to bio-based value-added chemicals: Modelling of mass transfer, thermodynamics and micro-kinetics, Chem. Eng. J. 330 (July) (2017) 383–397, https://doi.org/10.1016/j.cej.2017.07.145.

[33] W. Gao, R.L. Robinson, K.A.M. Gasem, High-pressure solubilities of hydrogen, nitrogen, and carbon monoxide in dodecane from 344 to 410 K at pressures to 13.2 MPa, J. Chem. Eng. Data 44 (1) (1999) 130–132, https://doi.org/10.1021/je9801664.

[34] V. Meille, N. Pestre, P. Fongarland, C. De Bellefon, Gas/liquid mass transfer in small laboratory batch reactors: comparison of methods, Ind. Eng. Chem. Res. 43 (4) (2004) 924–927, https://doi.org/10.1021/ie030569j.

[35] M.A. Matthews, J.B. Rodden, A. Akgerman, High-temperature diffusion of hydrogen, carbon monoxide, and carbon dioxide in liquid n-heptane, n-dodecane, and n-hexadecane, J. Chem. Eng. Data 32 (3) (1987) 319–322.

[36] T.M. Koller, T. Klein, C. Giraudet, J. Chen, A. Kalantar, G.P. van der Laan, M. H. Rausch, A.P. Fröba, Liquid viscosity and surface tension of n-dodecane, n-octacosane, their mixtures, and a wax between 323 and 573 K by surface light scattering, J. Chem. Eng. Data 62 (10) (2017) 3319–3333, https://doi.org/10.1021/acs.jced.7b00363.

[37] B. Hočevar, M. Grilc, M. Huš, B. Likozar, Mechanism, ab initio calculations and microkinetics of straight-chain alcohol, ether, ester, aldehyde and carboxylic acid hydrodeoxygenation over Ni-Mo catalyst, *Chem. Eng. J.*, 359(2018) (2019) 1339–1351, doi: 10.1016/j.cej.2018.11.045.

[38] J.I. del Río, F. Cardeño, W. Pérez, J.D. Peña, L.A. Rios, Catalytic hydrotreating of jatropha oil into non-isomerized renewable diesel: Effect of catalyst type and process conditions, Chem. Eng. J. 352 (June) (2018) 232–240, https://doi.org/10.1016/j.cej.2018.07.021.

[39] J. Sá, Y. Kayser, C.J. Milne, D.L. Abreu Fernandes, J. Szlachetko, Temperature-programmed reduction of NiO nanoparticles followed by time-resolved RIXS, Phys.

Chem. Chem. Phys. 16 (17) (2014) 7692–7696, https://doi.org/10.1039/c3cp54622e.
[40] M. Trueba, S.P. Trasatti, γ-alumina as a support for catalysts: A review of fundamental aspects, Eur. J. Inorg. Chem. 17 (2005) 3393–3403, https://doi.org/10.1002/ejic.200500348.
[41] C. Dupont, R. Lemeur, A. Daudin, P. Raybaud, Hydrodeoxygenation pathways catalyzed by MoS2 and NiMoS active phases: A DFT study, J. Catal. 279 (2) (2011) 276–286, https://doi.org/10.1016/j.jcat.2011.01.025.
[42] B. Hočevar, M. Grilc, M. Huš, B. Likozar, Mechanism, ab initio calculations and microkinetics of hydrogenation, hydrodeoxygenation, double bond migration and cis–trans isomerisation during hydrotreatment of C6 secondary alcohol species and ketones, Appl. Catal. B Environ. 218 (2017) 147–162, https://doi.org/10.1016/j.apcatb.2017.06.046.
[43] M.A.P. Pedroza, I.S.V. Segtovich, V.d.M. Sermoud, M.A.P. da Silva, Hydrodeoxygenation of stearic acid to produce diesel–like hydrocarbons: kinetic modeling, parameter estimation and simulation, Chem. Eng. Sci. 254 (2022) 117576, https://doi.org/10.1016/j.ces.2022.117576.
[44] R.V. Chaudhari, R.V. Gholap, G. Emig, H. Hofmann, Gas-liquid mass transfer in 'dead-end' autoclave reactors, Can. J. Chem. Eng. 65 (5) (1987) 744–751, https://doi.org/10.1002/cjce.5450650506.